Microgravity Science and Technology (2021) 33: 21
https://doi.org/10.1007/s12217-020-09864-2

ORIGINAL ARTICLE

Lattice Boltzmann Study on Influence of Gravitational Acceleration on Pool Nucleate Boiling Heat Transfer

Yuan Feng[1] · Huixiong Li[1] · Jianfu Zhao[2,3] · Kaikai Guo[1] · Xianliang Lei[1]

Received: 24 July 2020 / Accepted: 20 December 2020 / Published online: 5 March 2021

Abstract

Under both normal gravity and microgravity conditions, pool boiling is an efficient mode of heat transfer which has been widely applied in practice. Studying the influence of gravitational acceleration on boiling heat transfer is not only of academic significance, but also helpful for the design of space equipment related to boiling. With the development of computer technology, numerical method has been a new reliable way to investigate the boiling heat transfer under different gravities. Pseudopotential lattice Boltzmann (i.e., LB) model is one of the most popular multiphase LB models, in which the phase interface could be formed, disappeared and migrated naturally. In this paper, the Multi-Relaxation-Time (i.e., MRT) pseudopotential LB model coupled with phase-change model was applied to simulate the pool boiling heat transfer under different gravitational accelerations and wall superheats. Pool boiling curves under different gravities were obtained. It's found that: 1) the pool boiling heat transfer coefficient at a given wall superheat decreases with a decrease in gravity; 2) the wall superheat, as well as heat flux, at the CHF (i.e., critical heat flux) point and ONB (i.e., onset of the nucleate boiling) decrease gradually with a decrease in gravity. In addition, based on the numerical results, a new gravity scaling model was proposed to predict the influence of gravitational acceleration on the nucleate boiling heat transfer under different wall superheats. Finally, the new gravity scaling model was proved to be capable of predicting the heat flux during the nucleate boiling under different wall superheats and gravities.

Keywords Lattice Boltzmann method · Pool boiling heat transfer · Gravity scaling model

Highlights
1) Simulations of pool boiling processes at different gravity levels were performed.
2) Wall superheat and heat flux at ONB decreased with a decrease in gravity.
3) Wall superheat at CHF point and CHF decreased with a decrease in gravity.
4) A new scaling model for the nucleate boiling heat transfer was proposed.

✉ Huixiong Li
huixiong@mail.xjtu.edu.cn

✉ Jianfu Zhao
jfzhao@imech.ac.cn

[1] State Key Laboratory of Multiphase Flow in Power Engineering, Xi'an Jiaotong University, Xi'an 710049, China

[2] CAS Key Laboratory of Microgravity, Institute of Mechanics, Chinese Academy of Sciences, Beijing 100190, China

[3] School of Engineering Science, University of Chinese Academy of Sciences, Beijing 100049, China

Introduction

Boiling is a complex physical phenomenon, in which various physical components are involved and interrelated, such as the nucleation, growth, departure, and coalescence of vapor bubbles, the transport of latent heat, and the instability of liquid-vapor interfaces. At the same time, since the nucleate boiling has high heat transfer efficiency and can reach high heat flux at a low wall superheat, it is widely applied in practice under both normal gravity and microgravity conditions. Due to the large density ratio between the liquid and vapor, gravitational acceleration could affect the bubble dynamics and heat transfer during pool boiling processes. Studying the influence of gravitational acceleration on boiling heat transfer is not only of academic significance, but also helpful for the design of space equipment related to boiling and ensuring the safe operation of space system. Therefore, the researches of the mechanism of gravity on boiling phenomenon have become the frontier of microgravity research and have been paid close attention by many scholars.

Abundant experiments were carried out, lots of experimental data were obtained and boiling heat transfer theories were

proposed in the last one century. Using water as a working medium, Siegel et al. (Siegel and Keshock 1964) experimentally studied the bubble dynamics during nucleate boiling under microgravity. Using R113 as a working medium, Lee et al. (Lee et al. 1997) performed experiments on the pool boiling processes under microgravity conditions and studied the influence of gravity on boiling curves. They found that: 1) the heat transfer efficiency of steady nucleate boiling under microgravity is higher than that under normal gravity; 2) surface tension plays an important role in the drying and rewetting of heated surface; 3) the heat flux under microgravity when drying occurs is much smaller than that under normal gravity. Using FC-72 as a working medium, Kim et al. (Kim et al. 2002) investigated the boiling processes on a small heated surface under microgravity, normal gravity and hypergravity conditions. The growth of vapor bubbles during pool boiling was observed, and the influence of gravity and subcooling degree on boiling heat transfer performance was investigated. Kim et al. (Kim et al. 2002) found that critical heat flux decreases greatly under microgravity, while critical heat flux increases with an increase in subcooling degree. Using FC-72 as a working medium, Zhao et al. (Zhao et al. 2009) observed the growth of vapor bubbles on a horizontal heated wall in a retrievable scientific research satellite SJ-8, and they found that the boiling heat transfer and critical heat flux under microgravity increase with an increase in subcooling degree or pressure. However, the critical heat flux under microgravity is only as small as 1/3 of that under normal gravity. In addition, Zhao et al. (Zhao et al. 2009) found that the nucleate boiling could take place at a lower wall superheat and lower heat flux under microgravity. Soon after, Zhao (Zhao 2010) compared the boiling curves obtained under microgravity with those obtained under normal gravity, and they pointed out that heat transfer deterioration would take place under microgravity. In SOBER-SJ10 (i.e., Single bubble pool boiling experiment aboard satellite SJ-10), using FC-72 as a working medium, Wu et al. (Wu et al. 2016) investigated the partial nucleate boiling on a horizontal heated wall under low wall superheats and microgravity, and they found that the heat transfer efficiency increases with an increase in subcooling degree when wall superheat is low. However, with an increase in heat flux, the influence of subcooling degree on heat transfer efficiency would be weaker. Nearest, using FC-72 as a working medium, Nejati et al. (Nejati et al. 2020) experimentally investigated the single bubble nucleate boiling under microgravity condition and studied the effect of the preheating time on the nucleation and behavior of the bubbles. Based on the experimental data of FC-22's the nucleate boiling under normal gravity and microgravity, Raj et al. (Raj et al. 2010; Raj et al. 2012; Raj et al. 2009; Raj et al. 2011) proposed a gravity scaling model (i.e., RKM model) that could accurately predict the influence of gravitational acceleration on the nucleate boiling heat transfer under different wall superheats (Du and Zhao 2019).

However, it's undeniable that there are some disadvantages for the experimental method to study the influence of gravitational acceleration on boiling heat transfer, and some drawbacks exist in the current boiling theories. At first, the time and economic cost of carrying out boiling experiments in space is extremely high. Secondly, most of the previous boiling theories were proposed based on the experimental results on ground, therefore it's difficult to treat the gravity as a truly independent variable (Du and Zhao 2019). Finally, there are some obvious defects in the existing gravity scaling models for nucleate boiling heat transfer, although they have high prediction rate. For example, in the RKM model, it's assumed that the wall superheats at the CHF (i.e., critical heat flux) point and ONB (i.e., onset of the nucleate boiling) are independent with gravitational acceleration. Obviously, this assumption is inconsistent with the experimental observation in Ref. (Zhao et al. 2009). Moreover, it was assumed that the gravity exponent of the critical heat flux equals 1/4 in the RKM model. This assumption obviously confused the definitions of different gravity scaling parameters when the wall superheat at the CHF point is dependent with the gravitational acceleration (Du and Zhao 2019).

With the development of computer technology, more and more scholars simulated the boiling processes using macroscopic computational fluid dynamics (i.e., CFD) methods and investigated the influencing mechanism of gravitational acceleration on boiling heat transfer based on the numerical results (Li et al. 2015a; Zhang et al. 2015; Lee and Nydahl 1989; Son and Dhir 1999; Ling et al. 2014; Aktinol and Dhir 2012; Pandey et al. 2017; Dhruv et al. 2019; Yi et al. 2019; Mukherjee and Dhir 2004; Guo et al. 2019). In addition, Rajan et al. (Rajan et al. 2019) simulated the single bubble growth in presence and absence of electric fields under gravity and microgravity conditions and they found that applied voltage of 5 kV could reduce the bubble departure time greater than 100 ms under the microgravity condition for non-wetting surfaces. These researches made important contributions to the study of gravity's influencing mechanism on boiling heat transfer. However, since traditional CFD methods were used, an initial distribution of phase interface must be set and the nucleate site density must be assumed in these simulations. Therefore, it's difficult to study the influence of gravity on boiling curves by the traditional CFD method.

Due to its mesoscopic properties, lattice Boltzmann method (i.e., LBM) has the advantages of both the macroscopic methods and the microscopic methods. In addition, it's easy to describe the interaction between fluid and the surrounding environment, deal with complex boundary conditions and implement parallel computing for LBM. Still now, LBM has been utilized to simulated two-phase flow phenomenon, and various multiphase LB models (Rothman and Keller 1988; Gunstensen et al. 1991; Shan and Chen 1993; Swift et al. 1995) have been proposed. Among them, the pseudopotential

model (Shan and Chen 1993) has received extensive attention. In this model, the phases are directly distinguished by densities, the phase interface could be formed, disappeared and migrated naturally, and the interaction between fluid particles could be described by the pseudopotential.

Compared with traditional CFD method and other multiphase LB models, the pseudopotential model can realize the bubble nucleation processes automatically when it is applied to simulate pool boiling. Therefore, there's no need to set the initial distribution of phase interface and assume the nucleate site density or bubble waiting time. Hazi and Markus (Hazi and Markus 2009) simulated the single bubble pool nucleate boiling based on two-dimensional (2D) pseudopotential model, and the influence of gravitational acceleration and contact angle on bubble departure diameter and bubble release frequency was studied. Based on the pseudopotential model, Gong and Cheng proposed an improved 2D numerical model to simulate the boiling phenomenon (Gong and Cheng 2012), and the growth and departure of a single bubble on a micro heater was simulated (Gong and Cheng 2013). The influence of gravitational acceleration, wall superheat and contact angle on bubble dynamics and heat transfer efficiency was studied by them. Soon after, Gong and Cheng (Gong and Cheng 2015) simulated the pool boiling processes on a small heater and studied the wettability on the growth of bubbles during boiling processes. Boiling curves were obtained by LBM for the first time. Latest, Gong and Cheng (Gong and Cheng 2017) simulated the pool boiling processes on an infinite heated surface, and compared some of their numerical results with theoretical correlations. Using the same numerical model, Ma et al. (Ma et al. 2017) simulated the saturated pool boiling processes under different gravitational accelerations and studied the influence of gravitational acceleration, wall superheat and heater's size on heat transfer performance. They found that the critical heat flux decreases greatly under microgravity. Li et al. (Li et al. 2015b) also simulated the pool boiling processes under different wall superheats by using the Multi-Relaxation-Time (i.e., MRT) pseudopotential model coupled with phase-change model, and the influence of wettability on boiling heat transfer. They found that the critical heat flux decreases with an increase in contact angle.

It can be concluded that the pseudopotential model has been applied successfully in the simulations of pool boiling. However, few scholars investigated the influence of gravitational acceleration on boiling heat transfer. Although the influence of gravitational acceleration on bubble departure diameter was studied by Hazi (Hazi and Markus 2009) and Gong (Gong and Cheng 2013), and the effect of gravity on boiling heat transfer was studied by Ma et al. (Ma et al. 2017), these authors just showed their numerical results but didn't process and analyze the simulated results further. In view of the disadvantages in previous experimental and numerical researches and gravity scaling models, the pool boiling processes under different gravitational accelerations were simulated by the MRT pseudopotential model coupled with the phase-change model. The influence of gravitational acceleration on wall superheats at ONB and CHF point were investigated and the influence of gravitational acceleration on boiling heat transfer performance under different wall superheats were analyzed. The boiling curves under different gravitational accelerations were obtained and a new gravity scaling model for the nucleate boiling heat transfer was proposed based on the numerical results. Finally, by using the experimental and numerical results of other scholars, the rationality of new gravity scaling model was validated.

Numerical Method

The MRT Pseudopotential Model

The MRT pseudopotential model was adopted to simulate the two-phase flow phenomenon. Using this model, the evolution of the distribution function of density, i.e., f_α, could expressed as Eqs. (1)~(2).

$$f_\alpha{}^*(\mathbf{x},t) = f_\alpha(\mathbf{x},t) - \left(\mathbf{M}^{-1}\mathbf{\Lambda}\mathbf{M}\right)_{\alpha\beta}\left(f_\beta - f_\beta{}^{eq}\right) + \Delta t F_\alpha{}' \quad (1)$$

$$f_\alpha(\mathbf{x}+\mathbf{e}_\alpha\Delta t, t+\Delta t) = f_\alpha{}^*(\mathbf{x},t) \quad (2)$$

where, Eq. (1) and Eq. (2) are the collision step and streaming step, respectively. Δt is the time step, $\mathbf{e}_\alpha$ is the lattice velocity along the α^{th} direction. $\mathbf{\Lambda}$ is a diagonal matrix consists with several relaxation times. $\mathbf{M}$ is the transfer matrix.

F_α' is the forcing term in the velocity space. Using the Exact-Difference-Method (i.e., EDM) forcing scheme proposed by Kupershtokh et al. (Kupershtokh et al. 2009), F_α' could be expressed as Eq. (3), where $\Delta\mathbf{u} = \mathbf{F}\Delta t/\rho$ and w_α is the weighting coefficient along the α^{th} direction. c_s is the speed of sound.

$$F_\alpha{}' = w_\alpha \Delta t\left\{\frac{\mathbf{e}_\alpha\cdot\mathbf{F}}{{c_s}^2} + \frac{[(\mathbf{u}+0.5\Delta\mathbf{u})\mathbf{F}+\mathbf{F}(\mathbf{u}+0.5\Delta\mathbf{u})]:(\mathbf{e}_\alpha\mathbf{e}_\alpha - {c_s}^2\mathbf{I})}{2{c_s}^4}\right\} \quad (3)$$

The D2Q9 model is adopted for the two-dimensional simulations. Thus, $\mathbf{e}_\alpha$, $\mathbf{M}$ and $\mathbf{\Lambda}$ could be expressed as Eqs. (4)~(6), and the weighting coefficients $w_0 = 4/9$, $w_{1-4} = 1/9$ and $w_{5-8} = 1/36$. The speed of sound, ${c_s}^2 = 1/3c^2$. $c = \Delta x/\Delta t$, and Δx is the spatial step. In this study, both time step Δt and spatial step Δx take the value of 1.

$$\mathbf{e}_\alpha = c\begin{bmatrix} 0 & 1 & 0 & -1 & 0 & 1 & -1 & -1 & 1 \\ 0 & 0 & 1 & 0 & -1 & 1 & 1 & -1 & -1 \end{bmatrix} \quad (4)$$

$$\mathbf{M}=\begin{bmatrix} 1 & 1 & 1 & 1 & 1 & 1 & 1 & 1 & 1 \\ -4 & -1 & -1 & -1 & -1 & 2 & 2 & 2 & 2 \\ 4 & -2 & -2 & -2 & -2 & 1 & 1 & 1 & 1 \\ 0 & 1 & 0 & -1 & 0 & 1 & -1 & -1 & 1 \\ 0 & -2 & 0 & 2 & 0 & 1 & -1 & -1 & 1 \\ 0 & 0 & 1 & 0 & -1 & 1 & 1 & -1 & -1 \\ 0 & 0 & -2 & 0 & 2 & 1 & 1 & -1 & -1 \\ 0 & 1 & -1 & 1 & -1 & 0 & 0 & 0 & 0 \\ 0 & 0 & 0 & 0 & 0 & 1 & -1 & 1 & -1 \end{bmatrix} \tag{5}$$

$$\mathbf{\Lambda}=diag\left(\tau_\rho^{-1},\tau_e^{-1},\tau_\varsigma^{-1},\tau_j^{-1},\tau_q^{-1},\tau_j^{-1},\tau_q^{-1},\tau_\nu^{-1},\tau_\nu^{-1}\right) \tag{6}$$

where the value of τ_ν is related to the kinematic viscosity of fluid, $\tau_\nu = \nu/c_s^2 + 0.5$.

Multiply Eq. (1) with **M**, Eq. (7) could be obtained.

$$\mathbf{m}^* = \mathbf{m}-\mathbf{\Lambda}(\mathbf{m}-\mathbf{m}^{eq}) + \Delta t\mathbf{S} \tag{7}$$

where $\mathbf{m} = \mathbf{Mf}$, $\mathbf{m}^{eq} = \mathbf{Mf}^{eq}$ and $\mathbf{m}^* = \mathbf{Mf}^*$. $\mathbf{m}^{eq}$ could be calculated by Eq. (8). **S** is the forcing term in the moment space, and it could be calculated by Eq. (9).

$$\mathbf{m}^{eq}=\rho\left(1,-2+3|\mathbf{u}|^2,1-3|\mathbf{u}|^2,u_x,-u_x,u_y,-u_y,u_x^2-u_y^2,u_xu_y\right)^T \tag{8}$$

$$\mathbf{S}=\begin{bmatrix}0 & 6\mathbf{v}\cdot\mathbf{F} & -6\mathbf{v}\cdot\mathbf{F} & F_x & -F_x & F_y & -F_y & 2(v_xF_x-v_yF_y) & v_xF_y+v_yF_x\end{bmatrix}^T \tag{9}$$

In Eq. (8), ρ and **u** are macroscopic density and velocity, respectively. It should be noted that **u** is not the real velocity of fluid, but **v** in Eq. (9) is. $\mathbf{v} = \mathbf{u} + \Delta\mathbf{u}/2 = \mathbf{u} + 0.5\mathbf{F}\Delta t/\rho$. **F** is the total force. In this study, the total force **F** consists of intermolecular interaction force $\mathbf{F}_m$, fluid-solid interaction force $\mathbf{F}_{ads}$ and buoyancy force $\mathbf{F}_g$. These forces could be calculated by Eqs. (10)~(12), respectively.

$$\mathbf{F}_m = -3G\psi(\mathbf{x})\sum_{\alpha=1}^{8} w_\alpha\psi(\mathbf{x}+\mathbf{e}_\alpha)\mathbf{e}_\alpha \tag{10}$$

$$\mathbf{F}_{ads} = -G_w\psi(\mathbf{x})\sum_{\alpha=1}^{8} w_\alpha\psi(\mathbf{x})s(\mathbf{x}+\mathbf{e}_\alpha)\mathbf{e}_\alpha \tag{11}$$

$$\mathbf{F}_g = (\rho-\rho_{ave})\mathbf{g} \tag{12}$$

In Eq. (10), G is the interaction strength. ψ is the pseudopotential and can be calculated by Eq. (13). In Eq. (11), G_w is the fluid-solid interaction strength which could tune the contact angle. $s(\mathbf{x} + \mathbf{e}_\alpha)$ is a switch function which equals 0 and 1 for fluid and solid, respectively. In Eq. (12), **g** is the gravitational acceleration and ρ_{ave} is the averaged density of the whole computational domain.

$$\psi=\sqrt{2\left|\frac{p_{EOS}-\rho c_s^2}{Gc^2}\right|} \tag{13}$$

where p_{EOS} is the prescribed non-ideal equation of state. In this study, the Peng-Robinson equation of state (P-R EOS) is utilized, as shown in Eqs. (14)~(15).

$$p_{EOS}=\frac{\rho RT}{1-b\rho}-\frac{a\varphi(T)\rho^2}{1+2b\rho-b^2\rho^2} \tag{14}$$

$$\varphi(T)=\left[1+\left(0.37464+1.54226\omega-0.26992\omega^2\right)\left(1-\sqrt{T/T_c}\right)\right]^2 \tag{15}$$

where T is the temperature of fluid, $a = 0.45724R^2T_c^2/p_c$, $b = 0.0778RT_c/p_c$. T_c and p_c are critical temperature and critical pressure, respectively. At given critical temperature and critical pressure, the critical density ρ_c could be obtained.

The pseudopotential model always suffers from thermodynamic inconsistency (Li et al. 2013). To solve this problem, the improved forcing scheme proposed by Li et al. (Li et al. 2013) is used for reference in this study, and the forcing scheme in Eq. (7) could be modified as Eq. (16), where σ is a parameter used to tune the mechanical stability condition.

$$\mathbf{S}_{mod}=\mathbf{S}+\left[0\frac{\sigma|\mathbf{F}_m|^2}{\Psi^2\Delta t\tau_e}-\frac{\sigma|\mathbf{F}_m|^2}{\Psi^2\Delta t\tau_\varsigma}0\,0\,0\,0\,0\right] \tag{16}$$

In addition, the method proposed in Ref. (Li and Luo 2013) is utilized to tune the surface tension. As a result, Eq. (7) should be modified as Eq. (17), where **C** is the source term to tune the surface tension and can be expressed as Eq. (18).

$$\mathbf{m}^* = \mathbf{m}-\mathbf{\Lambda}(\mathbf{m}-\mathbf{m}^{eq}) + \Delta t\mathbf{S}_{mod} + \mathbf{C} \tag{17}$$

$$\mathbf{C}=\left[0,\frac{3\left(Q_{xx}+Q_{yy}\right)}{2\tau_e},-\frac{3\left(Q_{xx}+Q_{yy}\right)}{2\tau_\varsigma},0,0,0,0,-\frac{Q_{xx}-Q_{yy}}{\tau_\nu},-\frac{Q_{xy}}{\tau_\nu}\right]^T \tag{18}$$

where Q_{xx}, Q_{xy} and Q_{yy} could be calculated by Eq. (19).

$$\mathbf{Q} = 1.5\kappa G\psi(\mathbf{x})\sum_{\alpha=1}^{8} w_\alpha[\psi(\mathbf{x}+\mathbf{e}_\alpha)-\psi(\mathbf{x})]\mathbf{e}_\alpha\mathbf{e}_\alpha \tag{19}$$

Phase-Change Model

The phase-change model adopted in this study is derived from local balance law for entropy, see Ref. (Li et al. 2015b; Li et al. 2018) for details. The energy equation with phase-change source term could be expressed as Eq. (20).

$$\frac{\partial T}{\partial t}+\mathbf{v}\cdot\nabla T=\frac{1}{\rho c_v}\nabla\cdot(\lambda\nabla T)-\frac{T}{\rho c_v}\left(\frac{\partial p_{EOS}}{\partial T}\right)_\rho\nabla\cdot\mathbf{v} \tag{20}$$

where λ is the heat conductivity, c_v is the specific heat. The finite-difference-method (FDM) is adopted to solve Eq. (20) in this study. Eq. (20) could be rewritten as Eq. (21), and the

right-hand side of Eq. (21) is defined as $K(T)$. The 2nd order Runge-Kutta scheme is adopted for time discretization, as shown in Eq. (22), where h_1 and h_2 could be calculated by Eq. (23).

$$\frac{\partial T}{\partial t} = -\mathbf{v}\cdot\nabla T + \frac{1}{\rho c_v}\nabla\cdot(\lambda\nabla T) - \frac{T}{\rho c_v}\left(\frac{\partial p_{\mathrm{EOS}}}{\partial T}\right)_{\rho}\nabla\cdot\mathbf{v} \equiv K(T) \quad (21)$$

$$T(t+\Delta t) = T(t) + 0.5\Delta t(h_1+h_2) \quad (22)$$

$$h_1 = K(T(t)), h_2 = K(T(t)+0.5\Delta t h_1) \quad (23)$$

Physical Model and Calculation Parameters

As shown in Fig. 1, a rectangular computational domain with a size of $L_x \times L_y = 390 \times 400$ is adopted in the simulations. The symmetric boundary condition is utilized at the left and right boundaries, while the non-slip boundary condition is adopted at the top and bottom boundaries. At the same time, the bottom boundary is set as the heated surface with a temperature of T_w. The Peng-Robinson EOS is adopted in the simulations with $a = 3/49$, $b = 2/21$, $R = 1$ and $\omega = 0.344$. According to the definition of parameters a and b, critical temperature T_c and critical pressure p_c could be calculated to be 0.109383 and 0.08935, respectively. Substitute the values of T_c and p_c into Eq. (14), it's obtained that the critical density $\rho_c = 2.52$. The initial setting of the computational domain is a saturated liquid ($0 < y < 250$) below its vapor ($250 \le y < L_y$) and the saturated temperature is $T_{sat} = 0.9T_c$, and the densities of liquid and vapor are $\rho_L = 5.9$ and $\rho_V = 0.58$, respectively. In Eq. (6), the relaxation times are set as $\tau_\rho = 1$, $\tau_e = 1.25$, $\tau_\varsigma = 1.25$, $\tau_j = 1$ and $\tau_q = 1/1.1$. In Eq. (10), the interaction strength is set as $G = -1$. In Eq. (11), the fluid-solid interaction strength is $G_w = -0.24$, and the corresponding contact angle is 27.3° (see Appendix).

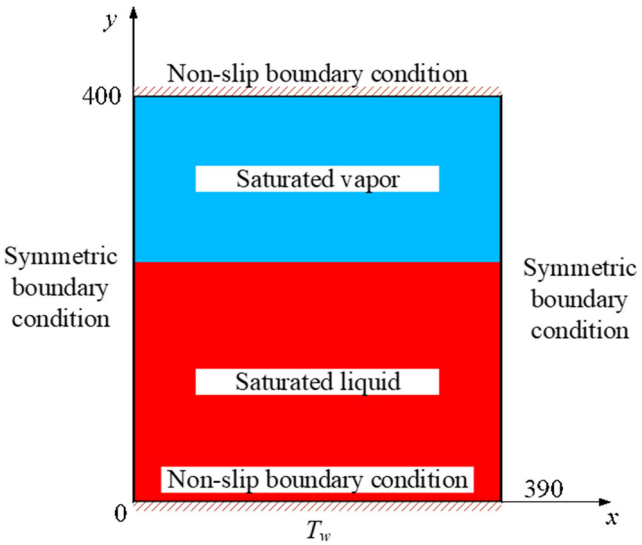

Fig. 1 The physical model of the simulations in this study

In Eq. (12), the gravitational acceleration is $\mathbf{g} = (0, -g)$. In Eq. (16), the parameter σ takes the value of 0.183. In Eq. (19), the parameter κ is set as 0.5, and the surface tension is set as $\gamma = 0.0748$ (see Appendix).

In this study, the characteristic length l_0, characteristic time t_0 and characteristic velocity v_0 are defined as Eq. (24), where the reference gravitational acceleration $g_0 = 5 \times 10^{-5}$. The dimensionless length l^*, dimensionless time t^* and dimensionless velocity $\mathbf{v}^*$ could be calculated by Eq. (25). In addition, Jacob number (Ja) is introduced to describe the wall superheat, as shown in Eq. (26). $Q_{loc}(x, t)$ is the local dimensionless heat flux at the heated surface, $Q_s(t)$ is the spatial average dimensionless heat flux of the heated surface and Q is the temporal and spatial average dimensionless heat flux, as shown in Eq. (27). The physical parameters used in the simulations and the unit conversion from lattice unit to physical unit are shown in Table 1. In addition, the simulations in this study were carried out under different gravitational accelerations within $g/g_0 \in [0.02, 1]$.

$$l_0 = \sqrt{\frac{\gamma}{g_0(\rho_L - \rho_V)}}, \quad v_0 = \sqrt{g_0 l_0}, \quad t_0 = \frac{l_0}{v_0} \quad (24)$$

$$l^* = l/l_0, \quad \mathbf{v}^* = \mathbf{v}/v_0, \quad t^* = t/t_0 \quad (25)$$

$$Ja = \frac{(T_w - T_{sat})}{h_{fg}} \quad (26)$$

$$Q_{loc}(x,t) = \frac{l_0(\lambda\Delta_y T)|_{y=0}}{\mu_L h_{fg}}, Q_s(t) = \frac{\int_{x=0}^{L_x} Q_{loc}(x,t)dx}{L_x}, Q_s(t) = \frac{\int_{t_1}^{t_2} Q_s(t)dt}{t_2 - t_1} \quad (27)$$

Results and Discussions

Pool Boiling Processes under Different Gravitational Accelerations

Figure 2 represents the bubble dynamics during pool boiling at $Ja = 0.136$ under different gravitational accelerations. As shown in Fig. 2a, there is no vapor bubble nucleated at the heated surface when $g/g_0 = 1$. In this case, the heat transfer mode of the heated surface is natural convection and the heat transfer coefficient is low. As shown in Fig. 2b, when $g/g_0 = 0.4$, vapor bubbles continuously nucleate on, grow on and depart away from the heated surface. However, due to the wall superheat is low, the growth and departure of each vapor bubble is independent and the interaction between vapor bubbles is weak. As shown in Fig. 2c, when $g/g_0 = 0.05$, compared with the pool boiling processes at $g/g_0 = 0.4$, the bubble size is increased obviously and the vapor bubble needs more time to depart away from the heated surface. With a decrease in

Table 1 The physical parameters used in the simulations

Physical parameters	Symbols	Lattice units	Physical units	Conversion factor
Reference gravitational acceleration	g_0	5×10^{-5}	9.8 m/s^2	1.96×10^5 m/s^2
Surface tension	γ	0.0748	0.1 N/m	1.337 N/m
Density of liquid	ρ_L	5.9	59 kg/m^3	10 kg/m^3
Density of vapor	ρ_V	0.58	5.8 kg/m^3	10 kg/m^3
Characteristic length	l_0	16.77	0.0138 m	8.26×10^{-4} m
Characteristic velocity	v_0	0.0290	0.368 m/s	12.69 m/s
Characteristic time	t_0	578.28	0.0375 s	6.48×10^{-5} s
Viscosity coefficient of liquid	ν_L	0.06	8.2×10^{-4} m^2/s	0.0137 m^2/s
Viscosity coefficient of vapor	ν_V	0.06	8.2×10^{-4} m^2/s	0.0137 m^2/s
Specific heat of liquid	$c_{v.L}$	6	211.94 J/kg·K	35.32 J/kg·K
Specific heat of vapor	$c_{v.V}$	1	35.32 J/kg·K	35.32 J/kg·K
Latent heat	h_{fg}	0.433	10,000 J/kg	2.31×10^4 J/kg
Thermal diffusion coefficient of liquid	χ_L	0.025	4.920×10^{-4} m^2/s	0.01968 m^2/s
Thermal diffusion coefficient of vapor	χ_V	0.03	5.904×10^{-4} m^2/s	0.01968 m^2/s
Heat conductivity of liquid	λ_L	0.885	6.152 W/m·K	6.952 W/m·K
Heat conductivity of vapor	λ_V	0.0174	0.121 W/m·K	6.952 W/m·K

gravitational acceleration, the width of vapor bubbles increases, and it's more likely for a vapor bubble to merge with other bubbles, as a result. In addition, it can be seen from Fig. 2 that the nucleate boiling could occur at a lower wall superheat under microgravity, and this result agrees well with the observation in the experiments of Zhao et al. (Zhao et al. 2009).

Figure 3 represents the bubble dynamics during pool boiling at Ja = 0.243 under different gravitational accelerations. As shown in Fig. 3a, when g/g_0 = 1, the pool boiling at the heated surface is in the nucleate boiling regime. Correspondingly, Fig. 4a shows the distribution of local heat flux of the heated surface (i.e., Q_{loc}). As shown in Fig. 4a, due to the nucleation and growth of vapor bubbles on the heated surface, the distribution of local heat flux is disturbed greatly. Near the liquid-vapor phase interface, Q_{loc} reaches its maximum value. However, at the dry area, Q_{loc} reaches its minimum value. In this case, the disturbance caused by the nucleation and growth of vapor bubbles benefits to enhance the boiling heat transfer.

As shown in Fig. 3b, at the case of g/g_0 = 0.05, since the bubble size is big before its departure and the nucleation site density is large, most of the area of the heated surface is dry area. Correspondingly, Fig. 4b shows the distribution of local heat flux of the heated surface. As shown in Fig. 4b, since the dry area is large and the thermal conductive of liquid is greater than that of vapor, the heat transfer performance in this case is poor. It can be inferred that the pool boiling in this case might be in the transition boiling regime.

As shown in Figs. 3 and 4, in the case of Ja = 0.243, with a decrease in gravitational acceleration, the pool boiling processes might be converted from the nucleate boiling to the transition boiling, indicating that the wall superheat at the CHF point shouldn't be independent with gravitational acceleration.

Figure 5 shows the bubble dynamics during pool boiling at Ja = 0.303 under different gravitational accelerations. As shown in Fig. 5a, when Ja = 0.303, abundant vapor bubbles are nucleated on the heated surface. Sometimes, vapor patches would occur at the heated surface due to the merging of the vapor bubbles. As a result, boiling heat transfer performance might be decreased and the pool boiling might be in the transition boiling regime. As shown in Fig. 5b, when g/g_0 = 0.05, due to the high wall superheat, a continuous vapor film is generated at the heated surface, which completely separates the heat transfer between heated surface and the bulk liquid. Obviously, the pool boiling in this case is in the film boiling regime. As shown in Fig. 5, under microgravity, since it's more difficult for the vapor bubbles to depart away from the heated surface, the pool boiling processes will enter into the film boiling regime at a lower wall superheat, which leads to severe heat transfer deterioration.

Rohsenow (Rohsenow 1951) proposed a correlation to predict the Nusselt number during nucleate boiling, as shown in Eq. (28), where C_{sf} is a undetermined parameter related to contact angle, Bo is the Bond number. Previous researches proved that Rohsenow's correlation could accurately predict the heat flux during the nucleate boiling with low wall superheat under normal gravity. According to the definition of Nusselt number, Eq. (29) could be used to calculate the dimensionless heat flux.

$$Nu_{Rohsenow} = \frac{Ja^2 Bo^{1/2}}{C_{sf}^3 \mathrm{Pr}_L^{4.1}} \tag{28}$$

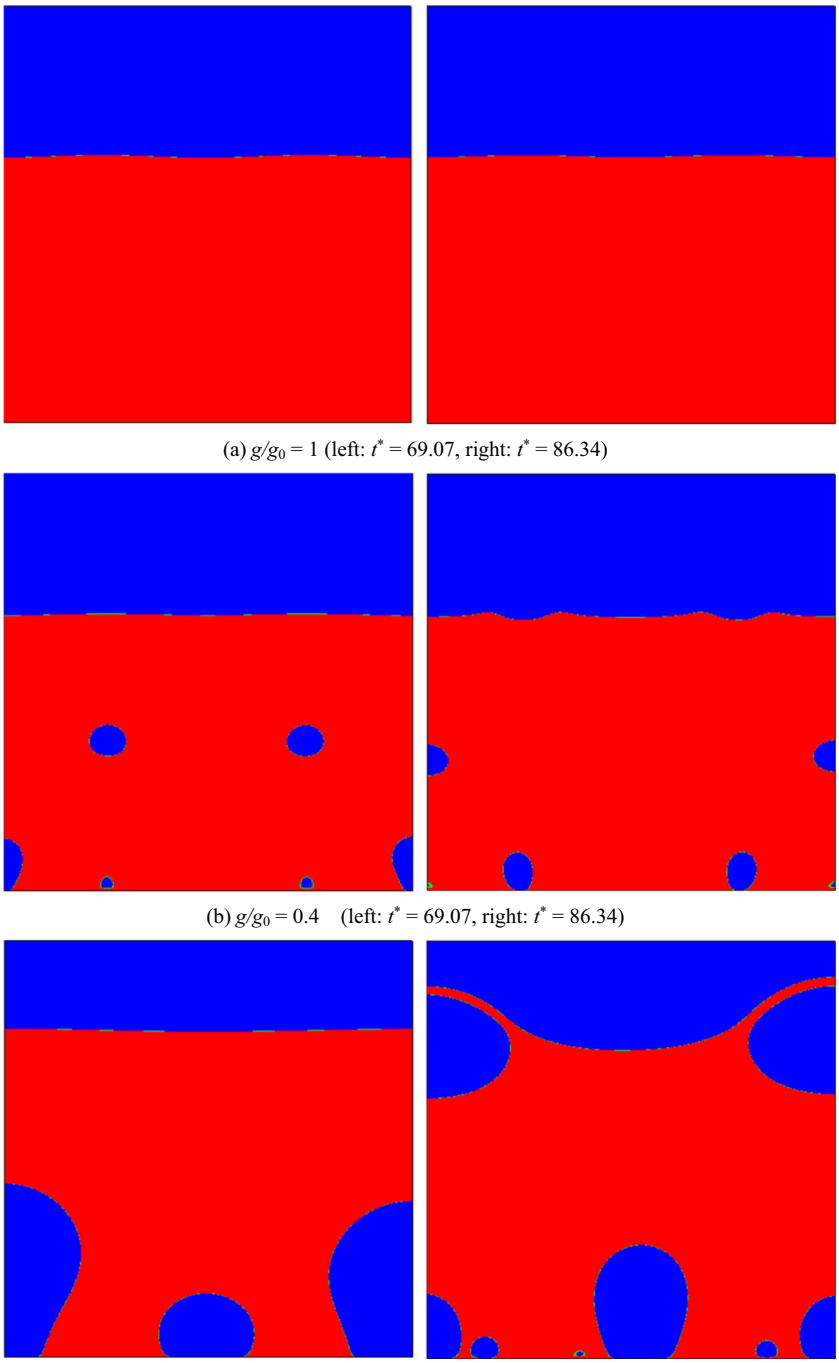

(a) $g/g_0 = 1$ (left: $t^* = 69.07$, right: $t^* = 86.34$)

(b) $g/g_0 = 0.4$ (left: $t^* = 69.07$, right: $t^* = 86.34$)

(c) $g/g_0 = 0.05$ (left: $t^* = 138.14$, right: $t^* = 207.21$)

Fig. 2 The bubble dynamics during pool boiling at $Ja = 0.136$ under different gravitational accelerations

$$Q_{Rohsenow} = \frac{Bo^{1/2}}{L_x^*}\left(\frac{Ja}{C_{sf}}\right)^3 \mathrm{Pr}_L^{-5.1} \tag{29}$$

In addition, the Nusselt number and heat flux of natural convection of a single phase fluid on a horizontal upward heated surface could be calculated by Eq. (30) (Incropera et al. 2007), where Gr is the Grashof number. When $10^4 \le Gr \le 10^7$, $\beta = 0.54$; when $10^7 \le Gr \le 10^{11}$, $\beta = 0.15$.

$$Nu_{NC} = \beta(Gr\mathrm{Pr})^{1/4}, \quad Q_{NC} = \beta\frac{\lambda\Delta T}{L_x^*\mu_L h_{fg}}(Gr\mathrm{Pr})^{1/4} \tag{30}$$

Figure 6 represents the influence of gravitational acceleration on boiling curves. As shown in Fig. 6, at a given gravitational acceleration, with an increase in wall superheat, the temporal and spatial average dimensionless heat flux Q increases at first and then decreases. After heat flux reaches its minimum value, it starts to increase slowly. According to the

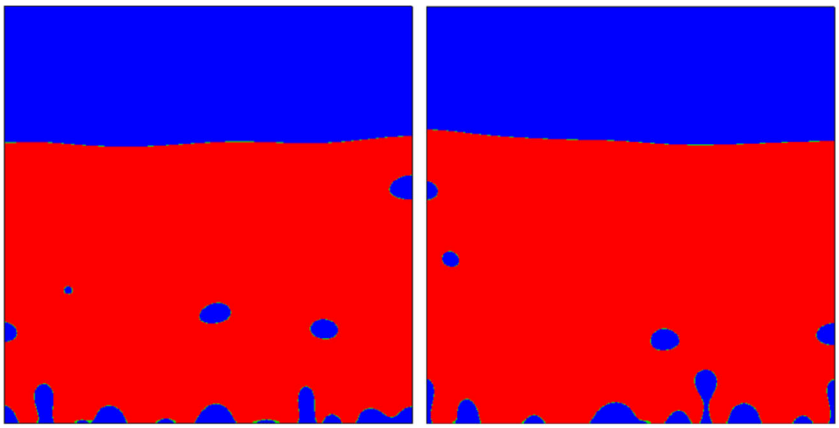

(a) $g/g_0 = 1$ (left: $t^* = 69.07$, right: $t^* = 86.34$)

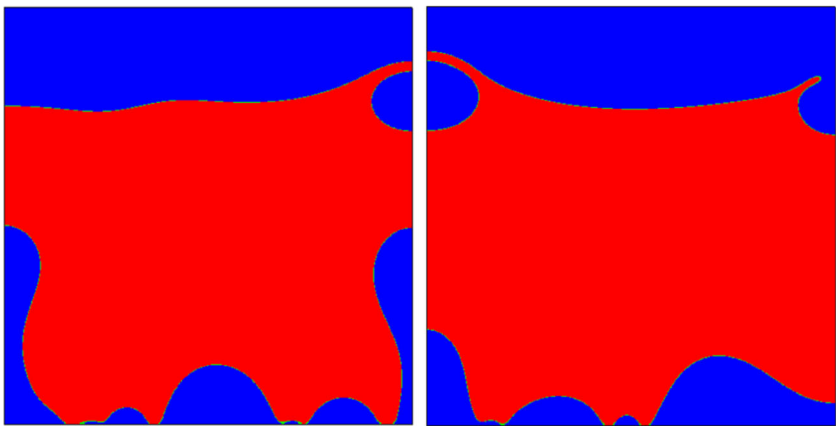

(b) $g/g_0 = 0.05$ (left: $t^* = 345.35$, right: $t^* = 414.42$)

Fig. 3 The bubble dynamics during pool boiling at $Ja = 0.243$ under different gravitational accelerations

variation tendency of Q, the regime of pool boiling heat transfer can be judged visually. It can be see also from Fig. 6 that the influence of gravitational acceleration on boiling heat transfer performance is weak when wall superheat is low. With an increase in wall superheat, the influence of gravitational acceleration on boiling heat transfer performance becomes greater. In addition, gravitational acceleration has a great impact on critical heat flux and the wall superheat at CHF point, as well. With a decrease in gravitational acceleration, CHF and the wall superheat at CHF point decrease obviously. At the same time, with a decrease in gravitational acceleration, pool boiling enters into the film boiling regime at a lower wall superheat. Moreover, for the film boiling at the same wall superheat, heat flux decreases with a decrease in gravitational acceleration. The predicted results of Eq. (30) and Rohsenow's correlation (Rohsenow 1951) when $C_{sf} = 0.0082$ are also given in Fig. 6. It can be seen that in the natural convection stage and the nucleate boiling regime with low wall superheat ($0.1516 \leq Ja \leq 0.2122$), under normal gravity, the numerical results obtained by present study agree well with the predicted results given by Eq. (30) and Rohsenow's correlation.

A New Gravity Scaling Model for the Nucleate Boiling Heat Transfer

In the previous boiling theories, it was assumed that the wall superheat and heat flux at the onset of nucleate boiling (ONB) is independent with gravitational acceleration. Previous gravity scaling models for nucleate boiling heat transfer were also proposed based on these assumptions (Raj et al. 2010). However, according to the experimental observation of Zhao et al. (Zhao et al. 2009), the nucleate boiling could take place at a lower temperature and heat flux under the microgravity conditions. Based on the numerical results obtained by present study, the influence of gravitational acceleration on wall superheat and heat flux at ONB (i.e., Ja_{ONB} and Q_{ONB}) is given in Fig. 7. In Fig. 7, $Ja_{ONB,0}$ and $Q_{ONB,0}$ represent the wall superheat and heat flux at ONB when $g/g_0 = 1$, respectively. As shown in Fig. 7, both Ja_{ONB} and Q_{ONB} decrease with a decrease in gravitational acceleration. This result is in agreement with the experimental results by Zhao et al. (Zhao et al. 2009) rather than the assumptions in previous boiling theories. In addition, it can be seen from Fig. 7 that with a decrease in in gravitational

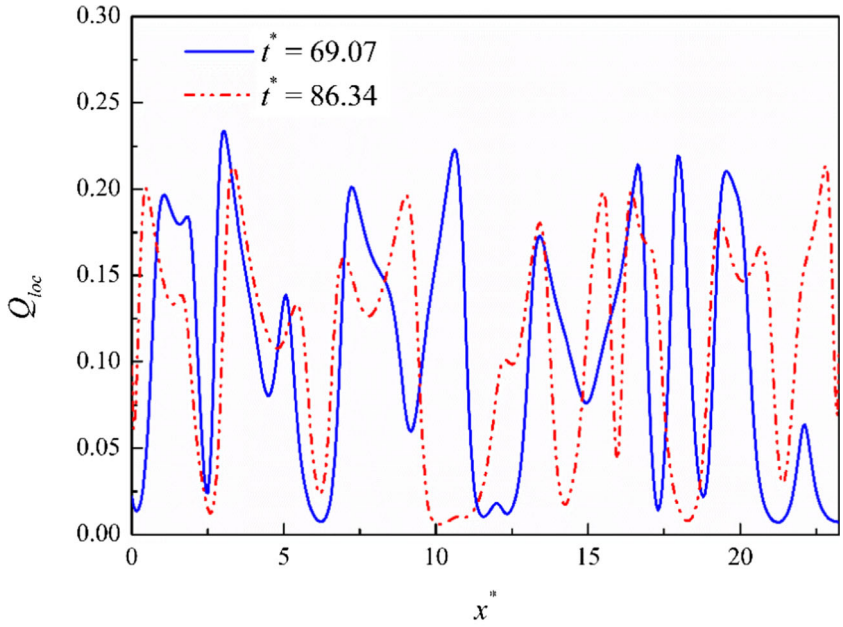

(a) $g/g_0 = 1$

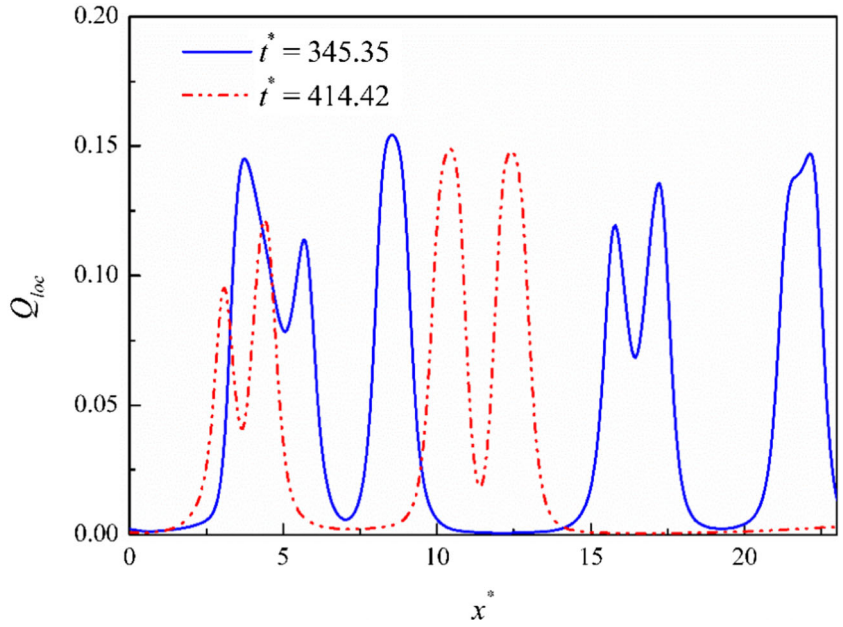

(b) $g/g_0 = 0.05$

Fig. 4 The distribution of local heat flux at the heated surface during the pool boiling processes at $Ja = 0.243$ under different gravitational accelerations

acceleration, both Ja_{ONB} and Q_{ONB} decrease rapidly when $0.3 \le g/g_0 \le 1$ but decrease slowly when $g/g_0 \le 0.2$. According to this rule, the quantitative relation between Ja_{ONB}, Q_{ONB} and gravitational acceleration could be fitted as Eqs. (31)~(32).

$$\frac{Ja_{ONB}}{Ja_{ONB,0}} = \begin{cases} 0.7098(g/g_0)^{0.006} & (g/g_0 < 0.2413) \\ (g/g_0)^{0.0448} & (0.2413 \le g/g_0 \le 1) \end{cases} \quad (31)$$

$$\frac{Q_{ONB}}{Q_{ONB,0}} = \begin{cases} 0.6196(g/g_0)^{0.0514} & (g/g_0 < 0.2413) \\ (g/g_0)^{0.3881} & (0.2413 \le g/g_0 \le 1) \end{cases} \quad (32)$$

Figure 8 represents the influence of gravitational acceleration on wall superheat and heat flux at CHF point (i.e., Ja_{CHF} and Q_{CHF}). In Fig. 8, $Ja_{CHF,0}$ and $Q_{CHF,0}$ are wall superheat and heat flux at CHF point when $g/g_0 = 1$, respectively. As shown in Fig. 8, Ja_{CHF} decreases with a decrease in gravitational acceleration, and this result is consistent with the numerical results of Ma et al. (Ma et al. 2017). The numerical results in Fig.

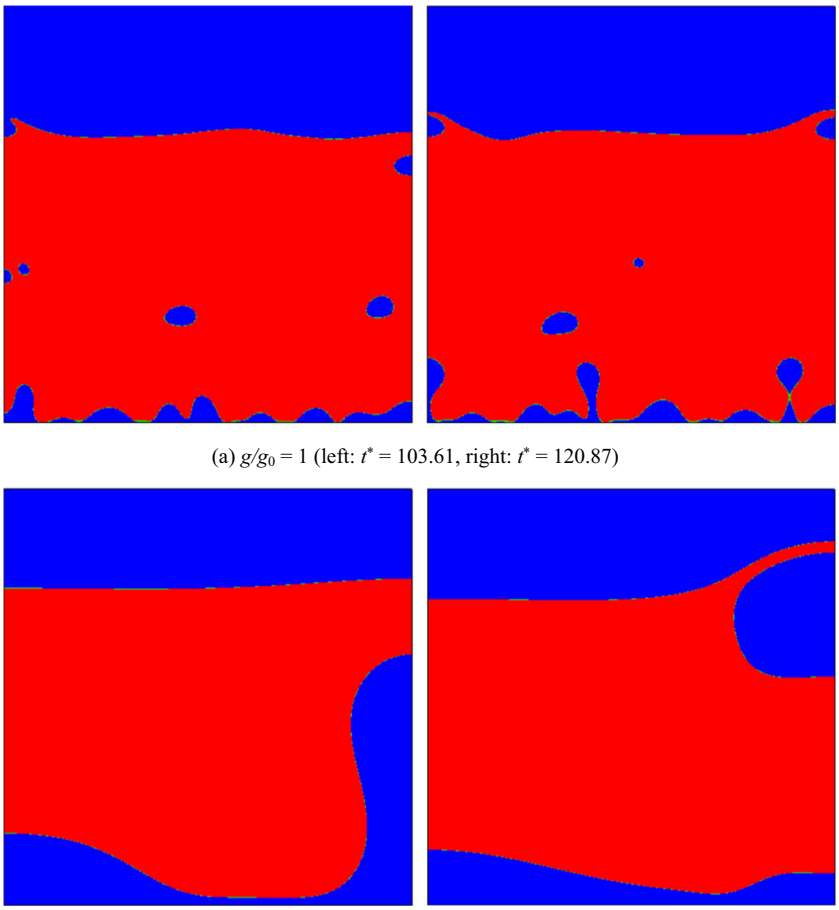

(a) $g/g_0 = 1$ (left: $t^* = 103.61$, right: $t^* = 120.87$)

(b) $g/g_0 = 0.05$ (left: $t^* = 103.61$, right: $t^* = 138.14$)

Fig. 5 The bubble dynamics during pool boiling at $Ja = 0.303$ under different gravitational accelerations

8 could be fitted as Eq. (33). Concretely, when $0.2413 \le g/g_0 \le 1$, the wall superheat at the CHF point is proportional to $g^{0.1325}$. When $g/g_0 < 0.2413$, the wall superheat at the CHF point is proportional to $g^{0.056}$. Combine Rohsenow's correlation for the nucleate boiling heat transfer (Rohsenow 1951) with Zuber's correlation for critical heat flux (Zuber 1959), it can be obtained that Ja_{CHF} is proportional to $g^{1/12}$, which is close to our numerical results. In addition, it can be seen from Fig. 8 that Q_{CHF} decreases with a decrease in gravitational acceleration, as well. Based on the numerical results in Fig. 8, Eq. (34) could be obtained. Concretely, when $0.2413 \le g/g_0 \le 1$, critical heat flux

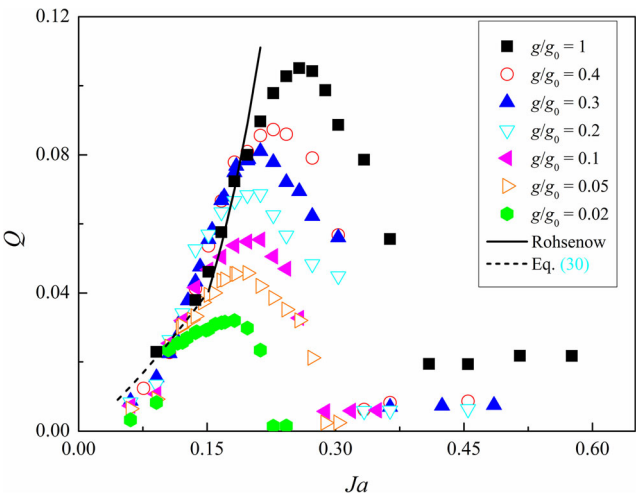

Fig. 6 The boiling curves under different gravitational accelerations

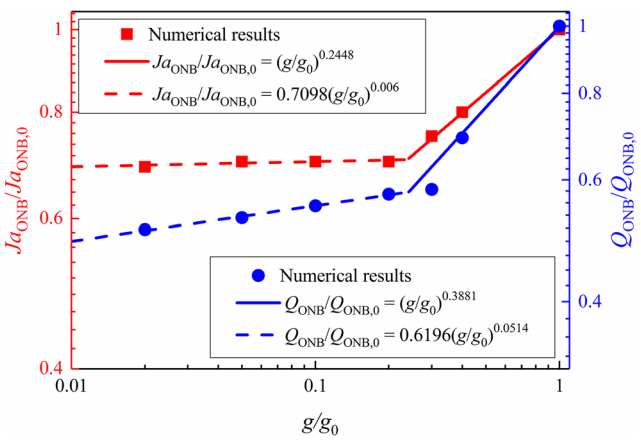

Fig. 7 The influence of gravitational acceleration on wall superheat and heat flux at ONB

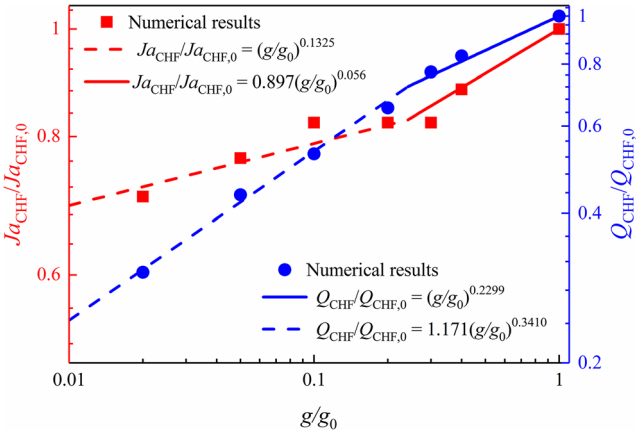

Fig. 8 The influence of gravitational acceleration on critical heat flux and wall superheat at CHF point

is proportional to $g^{0.2299}$, which is consistent with the predicted results by Zuber's correlation (Zuber 1959) and Kandlikar's correlation (Kandlikar 2001). When $g/g_0 < 0.2413$, critical heat flux is proportional to $g^{0.3410}$.

$$\frac{Ja_{CHF}}{Ja_{CHF,0}} = \begin{cases} 0.897(g/g_0)^{0.056} & (g/g_0 < 0.2413) \\ (g/g_0)^{0.1325} & 0.2413 \le g/g_0 \le 1 \end{cases} \quad (33)$$

$$\frac{Q_{CHF}}{Q_{CHF,0}} = \begin{cases} 1.171(g/g_0)^{0.3410} & (g/g_0 < 0.2413) \\ (g/g_0)^{0.2299} & 0.2413 \le g/g_0 \le 1 \end{cases} \quad (34)$$

Based on the numerical results, a new gravity scaling model to describe the influence of gravity on the nucleate boiling heat transfer under different wall superheats is proposed in this study. At first, a dimensionless temperature T^* is introduced, as shown in Eq. (35). Being different with that in the RKM model, Ja_{ONB} and Ja_{CHF} in Eq. (35) are related with gravitational acceleration, as shown in Figs. 7 and 8.

$$T^* = \frac{Ja - Ja_{ONB}(g)}{Ja_{CHF}(g) - Ja_{ONB}(g)} \quad (35)$$

Since the influence of gravitational acceleration on the wall superheat and heat flux at ONB and CHF point is significantly different between the regions of $0.2413 \le g/g_0 \le 1$ and $g/g_0 < 0.2413$, it's necessary to investigate the influence of T^* on nucleate boiling heat transfer in these two regions, respectively.

Figure 9a represents the influence of T^* on the value of $[\lg(Q/Q_0) - \lg A]/\lg(g/g_0)$ under different gravitational accelerations within $g/g_0 < 0.2413$, where $Q_0 = Q_0(T^*)$ represents the nucleate boiling heat flux at a given T^* under normal gravity ($g/g_0 = 1$). The definition of parameter A is expressed as Eq. (36). As shown in Fig. 9a the value of $[\lg(Q/Q_0) - \lg A]/\lg(g/g_0)$ is almost independent with gravitational acceleration in the region of $g/g_0 < 0.2413$. In addition, it can be seen from Fig. 9a that with an increase in T^*, the value of $[\lg(Q/Q_0) - \lg A]/\lg(g/g_0)$ increases obviously when $0 \le T^* < 0.4286$, while it increases slowly when $0.5714 \le T^* \le 1$. Based on the numerical results in Fig. 9a, the gravity scaling model for nucleate boiling heat transfer within $g/g_0 < 0.2413$ could be obtained, as shown in Eq. (37). Figure 9b represents the influence of dimensionless temperature T^* on the value of $\log_{(g/g0)}(Q/Q_0)$ under different gravitational accelerations within $0.2413 \le g/g_0 \le 1$. As shown in Fig. 9b, it can be approximately considered that the value of $\log_{(g/g0)}(Q/Q_0)$ is independent with gravitational acceleration within $0.2413 \le g/g_0 \le 1$. In addition, with an increase in T^*, the value of $\log_{(g/g0)}(Q/Q_0)$ decreases gradually when $0 \le T^* < 0.502$, while it stays almost unchanged when $0.502 \le T^* \le 1$. Using the numerical results in Fig. 9b, the gravity scaling model for the nucleate boiling heat transfer within $0.2413 \le g/g_0 \le 1$ could be obtained, as shown in Eq. (38).

$$A = \begin{cases} 1.281T^{*2} + 0.5556T^* + 0.6196 & 0 \le T^* < 0.502 \\ 1.18 & 0.502 \le T^* \le 1 \end{cases} \quad (36)$$

$$\frac{Q}{Q_0} = \begin{cases} (1.281T^{*2} + 0.5556T^* + 0.6196)(g/g_0)^{0.53T^* + 0.0501} & 0 \le T^* < 0.502 \\ 1.181(g/g_0)^{0.08T^* + 0.2759} & 0.502 \le T^* \le 1 \end{cases} \quad (37)$$

$$\frac{Q}{Q_0} = \begin{cases} (g/g_0)^{-0.472T^* + 0.435} & 0 \le T^* < 0.502 \\ (g/g_0)^{0.1981} & 0.502 \le T^* \le 1 \end{cases} \quad (38)$$

Combining Eq. (37) with Eq. (38), the complete gravity scaling model for nucleate boiling heat transfer is proposed in this paper, as shown in Eq. (39), where the parameters C and m could be calculated by Eq. (40) and Eq. (41), respectively.

$$\frac{q_w}{q_w(g/g_0) = 1} = C(g/g_0)^m \quad (39)$$

$$C = \begin{cases} 1 & 0.2413 \le g/g_0 \le 1 \\ 1.281T^{*2} + 0.5556T^* + 0.6196 & g/g_0 \le 0.2413 \& 0 \le T^* < 0.502 \\ 1.18 & g/g_0 \le 0.2413 \& 0.502 \le T^* \le 1 \end{cases} \quad (40)$$

$$m = \begin{cases} -0.472T^* + 0.435 & 0.2413 \le g/g_0 \le 1 \& T^* < 0.502 \\ 0.1981 & 0.2413 \le g/g_0 \le 1 \& T^* \ge 0.502 \\ 0.53T^* + 0.501 & g/g_0 < 0.2413 \& T^* < 0.502 \\ 0.08T^* + 0.2759 & g/g_0 < 0.2413 \& T^* < 0.502 \end{cases} \quad (41)$$

The Validation of the New Gravity Scaling Model Proposed in this Study

Comparison with Numerical Results

To validate the new gravity scaling model, the pool boiling heat transfer under different wall superheats when $g/g_0 = 0.6$

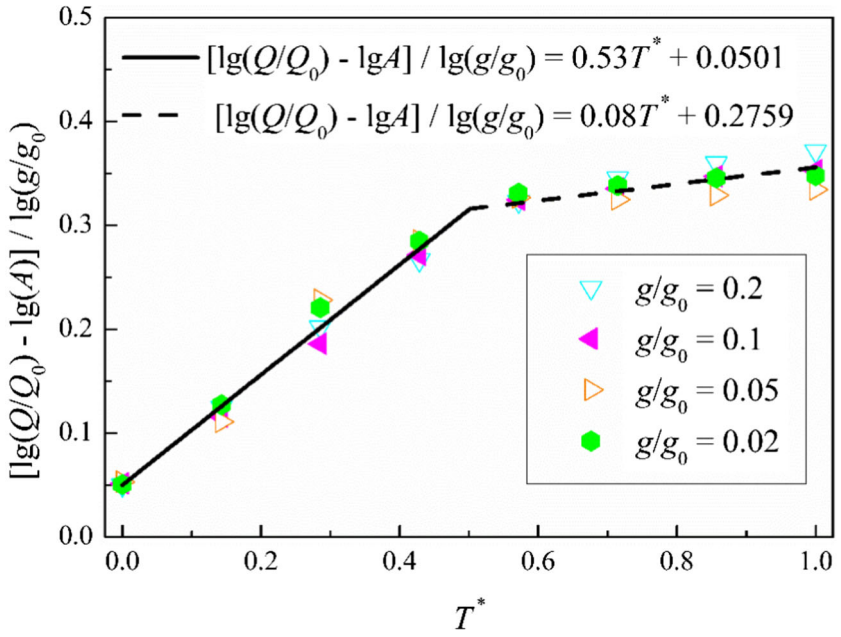

(a) $[\lg(Q/Q_0) - \lg A]/\lg(g/g_0)$ versus T^* when $g/g_0 < 0.2413$

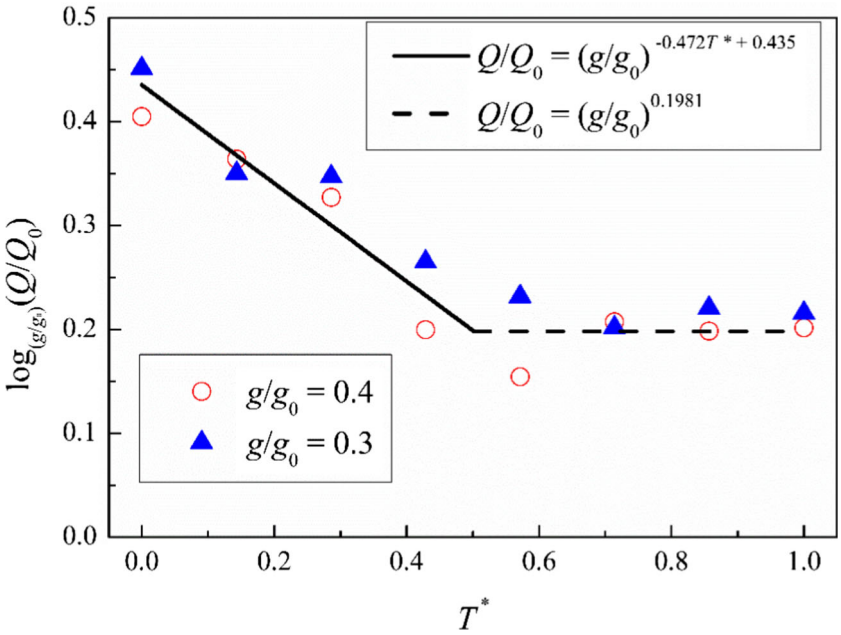

(b) $\log_{(g/g0)}(Q/Q_0)$ versus T^* when $0.2413 \le g/g_0 \le 1$

Fig. 9 The influence of dimensionless temperature T^* on Q/Q_0

and 0.035 are simulated extra at present study, and the numerical results are given in Fig. 10. To test whether Eqs. (31)~(34) could predict the wall superheats and heat fluxes at ONB and CHF point under different gravitational accelerations, the numerical results in Fig. 10 are compared with the predicted results by Eqs. (31)~(34), as shown in Table 2. It can be seen from Table 2 that all of these Ja_{ONB}, Q_{ONB}, Ja_{CHF} and Q_{CHF} predicted by Eqs. (31)~(34) agree well with our numerical results under different gravitational accelerations. The consistency between the predicted results and the numerical results could prove that Eqs. (31)~(34) could accurately predict the wall superheats and heat fluxes at ONB and CHF point under different gravitational accelerations.

Figure 11 displays the comparison between our numerical results with the predicted results given by Eq. (39) when g/g_0 = 0.6 and 0.035. In this figure, Q_{num} represents the simulated heat

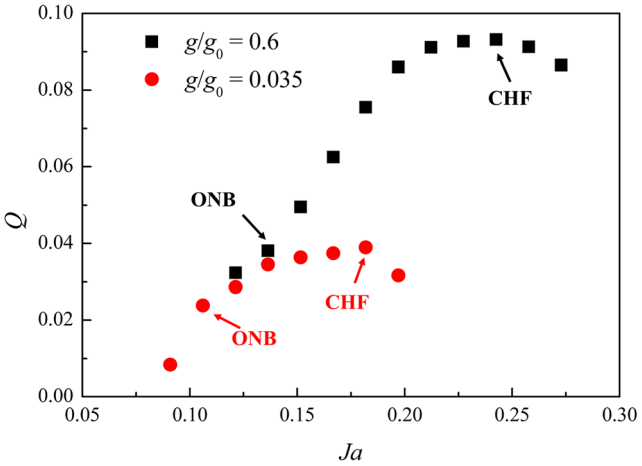

Fig. 10 The boiling curves at $g/g_0 = 0.6$ and 0.035

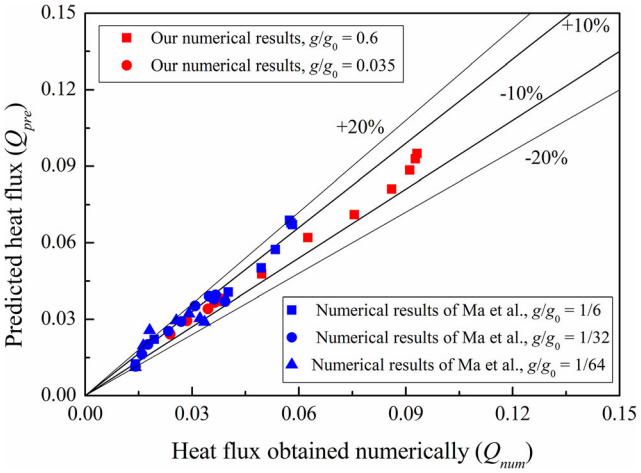

Fig. 11 The comparison between the numerical results with the predicted results given by the present gravity scaling model

flux during the nucleate boiling, Q_{pre} represents the predicted heat flux given by Eq. (39). As shown in Fig. 11, when $g/g_0 = 0.6$, the maximum deviation of 7.7% occurs at $Q_{num} = 0.0625$. When $g/g_0 = 0.035$, the maximum deviation of 2.9% occurs at $Q_{num} = 0.0390$. In sum, in both cases, the deviation between our numerical results and the predicted results is within 10% under all cases.

In addition, Fig. 11 also gives the comparison between the numerical results of Ma et al. (Ma et al. 2017) with the predicted results given by the present gravity scaling model. As shown in Fig. 11, when $g/g_0 = 1/6$, Q_{pre} is slightly greater than Q_{num}, and the maximum deviation of 19.9% occurs at $Q_{num} = 0.0574$. When $g/g_0 = 1/32$, the maximum deviation of 18.6% occurs at $Q_{num} = 0.0141$. When $g/g_0 = 1/64$, the maximum deviation of 41.9% occurs at $Q_{num} = 0.0181$. In sum, the deviation between the predicted results given by Eq. (39) and the numerical results in Ref. (Ma et al. 2017) is within 20% under different gravitational accelerations. Through the comparison between the predicted results given by Eq. (39) with the numerical results of both present study and Ma et al. (Ma et al. 2017), the rationality of the present gravity scaling model could be proved further.

Comparison with Experimental Results and the Predicted Results by RKM Model

Using the experimental results of Kim et al. (Kim et al. 2002), the 3D numerical results of Dhruv et al. (Dhruv et al. 2019) and the predicted results by RKM model (Raj et al. 2010; Raj et al. 2012; Raj et al. 2009; Raj et al. 2011), the present gravity scaling model is validated further. Using FC-72 as a working medium, Kim et al. (Kim et al. 2002) experimentally studied the influence of gravitational acceleration on bubble dynamics and heat transfer during pool boiling. Figure 12 gives the experimental results of Kim et al. (Kim et al. 2002) about the influence of gravitational acceleration on heat flux ratio Q/Q_0, in which the wall superheat is 34 K and the subcooling degree is 8 K. At the same time, the 3D numerical results of Dhruv et al. (Dhruv et al. 2019), the predicted results by RKM model (Raj et al. 2010; Raj et al. 2012; Raj et al. 2009; Raj et al. 2011) and the predicted results of the present model are also given in Fig. 12. As shown in Fig. 12, within $0.1 \le g/g_0 \le 1$, the present gravity scaling model is capable of predicting the influence of gravitational acceleration on heat flux ratio Q/Q_0 under a given wall superheat. The maximum deviation between the predicted results of present model and the experimental results is 17.6%. In addition, compared with the RKM model, the influencing tendency of gravitational acceleration on heat flux ratio predicted by present model is more consistent with the experimental results. However, the predicted results by present model are smaller than the experimental results of Kim et al. (Kim et al. 2002) and the 3D numerical results of Dhruv et al. (Dhruv et al. 2019). It's might because

Table 2 The wall superheats and heat fluxes at ONB and CHF point under different gravitational accelerations

	$g/g_0 = 0.6$			$g/g_0 = 0.035$		
	Numerical	Predicted	Deviations	Numerical	Predicted	Deviations
Ja_{ONB}	0.1364	0.1338	−1.91%	0.1061	0.1054	−0.66%
Q_{ONB}	0.0381	0.0378	−0.79%	0.0238	0.0241	1.26%
Ja_{CHF}	0.2425	0.2408	−0.70%	0.1819	0.1916	5.33%
Q_{CHF}	0.0931	0.0934	0.32%	0.0389	0.0392	0.77%

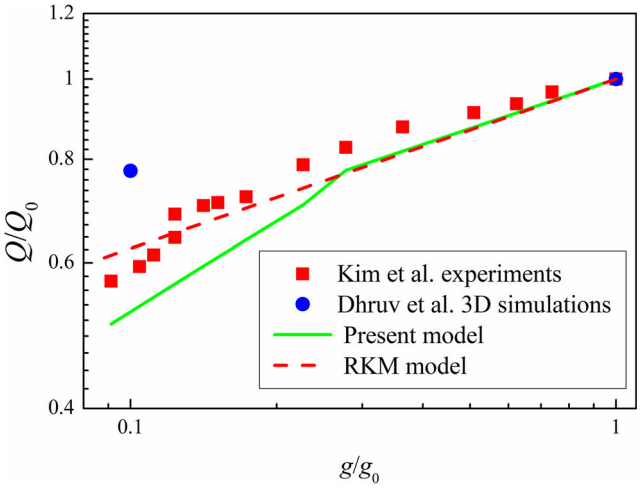

Fig. 12 The comparison between the predicted results given by the present model with the experimental results of Kim et al. (Kim et al. 2002), the 3D numerical results of Dhruv et al. (Dhruv et al. 2019) and the predicted results of RKM model

that the symmetric boundary condition is applied in our simulations, and the heated surface is infinite. As a result, the nucleation of small vapor bubbles at the boundaries is restrained, which would lead to a lower boiling heat transfer performance under microgravity. In our further work, we will simulate the pool boiling processes on a finite heated surface by LBM, study the influence of gravitational acceleration on boiling heat transfer and propose a more accurate gravity scaling model for nucleate boiling heat transfer.

Conclusion

In this study, the pool boiling processes under different wall superheats and gravitational accelerations were simulated based on the improved MRT pseudopotential model coupled with the phase-change model. The influence of

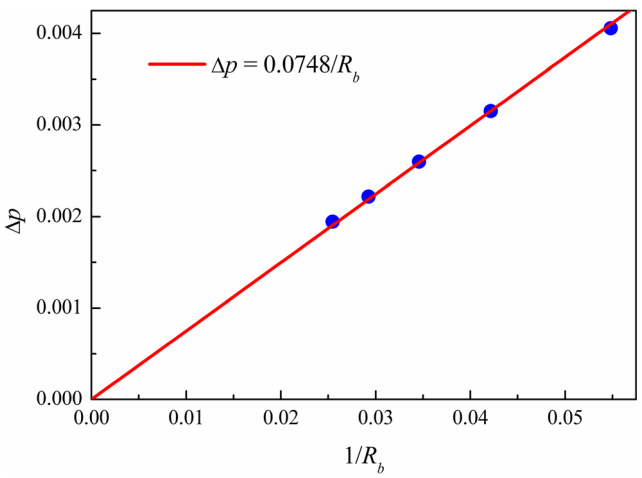

Fig. 13 The influence of droplet radii on the pressure difference

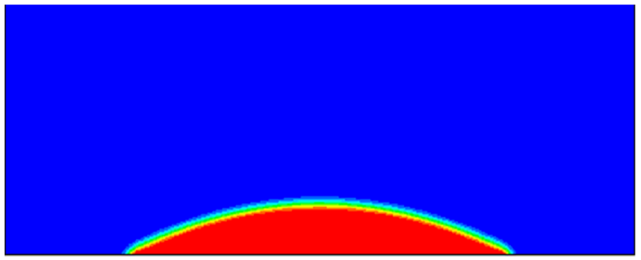

Fig. 14 The equilibrium shape of a droplet on the horizontal wall

gravitational acceleration on bubble dynamics and heat transfer performance during pool boiling was investigated. In addition, based on the numerical results, a new gravity scaling model was proposed in this paper to predict the nucleate boiling heat transfer performance under different gravitational accelerations and wall superheats. At last, using the experimental and numerical results of other scholars, the rationality of the present gravity scaling model was validated. It can be concluded that:

1) With a decrease in gravitational acceleration, the wall superheat at the ONB and the corresponding heat flux decrease fast at first, and then decrease slowly. Concretely, when $0.2413 \le g/g_0 \le 1$, Ja_{ONB} and Q_{ONB} are proportional to $g^{0.2448}$ and $g^{0.3881}$, respectively; when $g/g_0 < 0.2413$, Ja_{ONB} and Q_{ONB} are proportional to $g^{0.006}$ and $g^{0.0514}$, respectively.
2) With a decrease in gravitational acceleration, CHF and the wall superheat at CHF point decrease obviously. It means that at the same wall superheat, nucleate boiling might be converted into transition boiling or even film boiling due to the decreasing gravitational acceleration. Concretely, when $0.2413 \le g/g_0 \le 1$, Ja_{CHF} and Q_{CHF} are proportional to $g^{0.1325}$ and $g^{0.2299}$, respectively; when $g/g_0 < 0.2413$, Ja_{CHF} and Q_{CHF} are proportional to $g^{0.056}$ and $g^{0.3410}$, respectively.
3) The wall superheat at the minimum heat flux point of film boiling decreases with a decrease in gravitational acceleration, indicating that pool boiling enters into film boiling at a lower wall superheat under microgravity.
4) The new gravity scaling model for the nucleate boiling heat transfer proposed by present study is capable of predicting the heat flux during the nucleate boiling under different wall superheats and gravitational accelerations.

Acknowledgements This work was supported financially by the joint fund between the Chinese Academy of Sciences (CAS) and National Natural Science Foundation of China (NSFC) under the Grant of U1738105.

Nomenclature a,b,R,ω, parameters in EOS; T_{sat}, saturation temperature; c_v, specific heat at constant volume; T_w, temperature of the heated surface; $\mathbf{e}_\alpha$, lattice velocity vector; $\mathbf{u}$, fluid velocity; f_α, $\mathbf{f}$, distribution function for density; $\mathbf{v}$, real fluid velocity; $\mathbf{F}$, external force; v_0, characteristic velocity;

F_α', forcing term in the velocity space; w_α, weighting coefficient; $\mathbf{F}_{ads}$, fluid-solid interaction force; **x**, position; $\mathbf{F}_g$, buoyancy force; $\mathbf{F}_m$, intermolecular interaction force; **g**, gravitational acceleration; G, interaction strength**Greek Symbols** θ_w, contact angle; G_w, a parameter to tune the contact angle; Δt, time step; h_{fg}, latent heat of vaporization; ΔT, wall superheat; ρ, density; Ja, Jacob number; σ, parameter to tune the mechanical stability; l_0, characteristic length; L_x, width of computational domain; L_y, height of computational domain; **M**, orthogonal transformation matrix; p, pressure; p_c, critical pressure; p_{EOS}, prescribed non-ideal equation of state; R_b, liquid radius; $s(\mathbf{x})$, switch function; **S**, forcing term in the moment space; τ, relaxation time; χ, thermal diffusion coefficient; ν, kinematic coefficient of viscosity; γ, surface tension; **P**, pressure tensor; $\mathbf{\Lambda}$, diagonal matrix of relaxation time; $\mathbf{\Pi}$, viscous stress tensor; κ, parameter to tune the surface tension; μ, dynamic coefficient of viscosity; λ, thermal conductivity; ψ, pseudopotential; $Q_{loc}(x, t)$, local heat flux on the heated surface; $Q_s(t)$, space- averaged heat flux; Q, time- and space-averaged heat flux; t, time; t_0, characteristic time; T, temperature; T_c, critical temperature**Subscripts and Superscripts** *, dimensionless properties; α, lattice direction; c, critical properties; L, V, liquid, vapor; x, y, direction; eq, equilibrium properties

Appendix: the determination of surface tension and contact angle.

In the two-dimensional simulations, according to the Laplace equation of capillary, the relationship between the pressure difference across the interface of a droplet Δp and the radius of this droplet satisfies Eq. (A-1).

$$\Delta p = \frac{\gamma}{R_b} \qquad (A-1)$$

where γ is the surface tension. It can be seen from Eq. (A-1) that the pressure difference across the interface of the droplet is proportional to the inverse of droplet radius, and the proportionality coefficient equals to the surface tension.

To determine the surface tension in our simulations, the static droplets with different radii are simulated. In the simulations, a 120 × 120 computational domain is adopted and the periodic boundary condition is utilized at all of the boundaries. The static droplet is located at the center of the computational domain. All of the parameters in Peng-Robinson EOS, Eqs. (6), (10) and (19), and the physical parameters of fluid are chosen as those in Chapter 3. The fluid-solid interaction force and the buoyancy force are ignored. Figure 13 represents the influence of droplet radii on the pressure difference across the phase interface. As shown in Fig. 13, our numerical results could be fitted with a straight line that goes through the origin point with a slope of 0.0748. According to the Laplace equation of capillary, the surface tension could be determined as $\gamma = 0.0748$.

In order to determine the wettability of the heated surface in our simulations, the equilibrium shape of a droplet on the horizontal wall is simulated and the static contact angle is measured. In this simulation, a 300 × 100 computational domain is adopted. The periodic boundary condition is adopted at the left and right boundaries, while the non-slip boundary condition is utilized at the top and bottom boundaries. The parameters in P-R EOS, Eqs. (6), (10), (11) and (19) and the physical parameters of fluid are chosen as those in Chapter 3. The gravitational acceleration is set to be 0, so the buoyancy force is ignored. Initially, a droplet with a radius of $R_b = 30$ is located at (150, 20). The simulation is carried out for 10,000 time steps to ensure that the equilibrium state has been reached. As shown in Fig. 14, the static contact angle is measured to be 27.3°.

References

Aktinol, E., Dhir, V.K.: Numerical simulation of nucleate boiling phenomenon coupled with thermal response of the solid. Microgravity Sci Technol. **24**, 255–265 (2012)

Dhruv, A., Balaras, E., Riaz, A., Kim, J.: A formulation for high-fidelity simulations of pool boiling in low gravity. Int. J. Multiphase Flow. **120**, 103099 (2019)

Du, W., Zhao, J.: Gravity scaling law of heat transfer in nucleate pool boiling. Chin. Sci. Bull. (2019)

Gong, S., Cheng, P.: A lattice Boltzmann method for simulation of liquid–vapor phase-change heat transfer. Int. J. Heat Mass Transf. **55**, 4923–4927 (2012)

Gong, S., Cheng, P.: Lattice Boltzmann simulation of periodic bubble nucleation, growth and departure from a heated surface in pool boiling. Int. J. Heat Mass Transf. **64**, 122–132 (2013)

Gong, S., Cheng, P.: Lattice Boltzmann simulations for surface wettability effects in saturated pool boiling heat transfer. Int. J. Heat Mass Transf. **85**, 635–646 (2015)

Gong, S., Cheng, P.: Direct numerical simulations of pool boiling curves including heater's thermal responses and the effect of vapor phase's thermal conductivity. Int Commun Heat Mass Transfer. **87**, 61–71 (2017)

Gunstensen, A.K., Rothman, D.H., Zaleski, S., Zanetti, G.: Lattice Boltzmann model of immiscible fluids. **43**, 4320 (1991)

Guo, K., Li, H., Feng, Y., Zhao, J., Wang, T.: Numerical investigation on single bubble and multiple bubbles growth and heat transfer during flow boiling in a microchannel using the VOSET method. Microgravity Sci Technol. **31**, 381–393 (2019)

Hazi, G., Markus, A.: On the bubble departure diameter and release frequency based on numerical simulation results. Int. J. Heat Mass Transf. **52**, 1472–1480 (2009)

Incropera, F.P., Lavine, A.S., Bergman, T.L., DeWitt, D.P.: Fundamentals of Heat and Mass Transfer. Wiley (2007)

Kandlikar, S.G.: A theoretical model to predict Pool boiling CHF incorporating effects of contact angle and orientation. J. Heat Transf. **123**, 1071–1079 (2001)

Kim, J., Benton, J.F., Wisniewski, M.: Transfer, Pool boiling heat transfer on small heaters: effect of gravity and subcooling. **45**, 3919–3932 (2002)

Kupershtokh, A.L., Medvedev, D.A., Karpov, D.I.: On equations of state in a lattice Boltzmann method. Comput Math Appl. **58**, 965–974 (2009)

Lee, R.C., Nydahl, J.E.: Numerical calculation of bubble growth in nucleate boiling from inception through departure. J. Heat Transf. **111**, 474–479 (1989)

Lee, H.S., Herman, M., Jr Chiaramonte, H.: Transfer, Pool boiling curve in microgravity. **11**, 216–222 (1997)

Li, Q., Luo, K.H.: Achieving tunable surface tension in the pseudopotential lattice Boltzmann modeling of multiphase flows. Phys. Rev. E Stat. Nonlinear Soft Matter Phys. **88**, 053307 (2013)

Li, Q., Luo, K.H., Li, X.J.: Lattice Boltzmann modeling of multiphase flows at large density ratio with an improved pseudopotential model. Phys. Rev. E Stat. Nonlinear Soft Matter Phys. **87**, 053301 (2013)

Li, Z.-D., Zhang, L., Zhao, J.-F., Li, H.-X., Li, K., Wu, K.: Numerical simulation of bubble dynamics and heat transfer with transient thermal response of solid wall during pool boiling of FC-72. Int. J. Heat Mass Transf. **84**, 409–418 (2015a)

Li, Q., Kang, Q.J., Francois, M.M., He, Y.L., Luo, K.H.: Lattice Boltzmann modeling of boiling heat transfer: the boiling curve and the effects of wettability. Int. J. Heat Mass Transf. **85**, 787–796 (2015b)

Li, Q., Huang, J.Y., Kang, Q.J.: On the temperature equation in a phase change pseudopotential lattice Boltzmann model. Int. J. Heat Mass Transf. **127**, 1112–1113 (2018)

Ling, K., Li, Z.Y., Tao, W.Q.: A direct numerical simulation for nucleate boiling by the VOSET method, numerical heat transfer. Part A: Appl. **65**, 949–971 (2014)

Ma, X., Cheng, P., Gong, S., Quan, X.: Mesoscale simulations of saturated pool boiling heat transfer under microgravity conditions. Int. J. Heat Mass Transf. **114**, 453–457 (2017)

Mukherjee, A., Dhir, V.K.: Study of lateral merger of vapor bubbles during nucleate Pool boiling. J. Heat Transf. **126**, 1023–1039 (2004)

Nejati, I., Sielaff, A., Franz, B., Zimmermann, M., Hänichen, P., Schweikert, K., Krempel, J., Stephan, P., Martin, A., Scheerer, H., Engler, T., Oechsner, M.: Experimental investigation of single bubble nucleate boiling in microgravity. Microgravity Sci Technol. **32**, 597–607 (2020)

Pandey, V., Biswas, G., Dalal, A.: Saturated film boiling at various gravity levels under the influence of electrohydrodynamic forces. Phys. Fluids. **29**, 032104 (2017)

Raj, R., Kim, J., McQuillen, J.: Subcooled Pool boiling in variable gravity environments. J. Heat Transf. **131**, (2009)

Raj, R., Kim, J., McQuillen, J.: Gravity scaling parameter for Pool boiling heat transfer. J. Heat Transf. **132**, 091502–091509 (2010)

Raj, R., Kim, J., McQuillen, J.: On the scaling of Pool boiling heat flux with gravity and heater size. J. Heat Transf. **134**, (2011)

Raj, R., Kim, J., McQuillen, J.: Pool boiling heat transfer on the international Space Station: experimental results and model verification. J. Heat Transf. **134**, 101504–101514 (2012)

Rajan, V.K., Chandramouli, V., Seshadri, S., Muniyandi, V.: Electrohydrodynamic effects on single bubble growth and departure under microgravity conditions: a numerical investigation. Microgravity Sci Technol. **31**, 805–819 (2019)

Rohsenow, W.M.: A method of correlating heat-transfer data for surface boiling of liquids. Trans Asme. **74**, (1951)

Rothman, D.H., Keller, J.M.: Immiscible cellular-automaton fluids. J. Stat. Phys. **52**, 1119–1127 (1988)

Shan, X., Chen, H.: Lattice Boltzmann model for simulating flows with multiple phases and components. Phys Rev E Stat Phys Plasmas Fluids Relat Interdisc Topics. **47**, 1815–1819 (1993)

Siegel, R., Keshock, E.G.: Effects of reduced gravity on nucleate boiling bubble dynamics in saturated water. AICHE J. **10**, 509–517 (1964)

Son, G., Dhir, V.K.: Dynamics and heat transfer associated with a single bubble during nucleate boiling on a horizontal surface. J. Heat Transf. **121**, 623–631 (1999)

Swift, M.R., Osborn, W.R., Yeomans, J.M.: Lattice Boltzmann simulation of nonideal fluids. Phys. Rev. Lett. **75**, 830–833 (1995)

Wu, K., Li, Z.D., Zhao, J.F., Li, H.X., Li, K.: Partial nucleate Pool boiling at low heat flux: preliminary ground test for SOBER-SJ10. Microgravity Sci Technol. **28**, 165–178 (2016)

Yi, T.-H., Lei, Z.-S., Zhao, J.-F.: Numerical investigation of bubble dynamics and heat transfer in subcooling pool boiling under low gravity. Int. J. Heat Mass Transf. **132**, 1176–1186 (2019)

Zhang, L., Li, Z.-D., Li, K., Li, H.-X., Zhao, J.-F.: Influence of heater thermal capacity on bubble dynamics and heat transfer in nucleate pool boiling. Appl. Therm. Eng. **88**, 118–126 (2015)

Zhao, J.F.: Two-phase flow and pool boiling heat transfer in microgravity. Adv Mech. **36**, 135–143 (2010)

Zhao, J.F., Li, J., Yan, N., Wang, S.F.: Bubble behavior and heat transfer in quasi-steady pool boiling in microgravity. Microgravity Sci Technol. **21**, 175–183 (2009)

Zuber, N.: Hydrodynamic Aspects of Boiling Heat Transfer, In, Vol. Ph.D. University of California, Los Angeles (1959)